# Physics potential of timing layers for future detectors

C.-H. Yeh[a], S.V. Chekanov[b], A.V. Kotwal[c], N.V. Tran[d], S.-S. Yu[a]

[a] *Department of Physics and Center for High Energy and High Field Physics, National Central University, Chung-Li, Taoyuan City 32001, Taiwan*
[b] *HEP Division, Argonne National Laboratory, 9700 S. Cass Avenue, Argonne, IL 60439, USA.*
[c] *Department of Physics, Duke University, USA*
[d] *Fermi National Accelerator Laboratory*

**Abstract**

*Keywords:*

**Contents**



## 1. Introduction

Future experiments, such as CLIC [**?** ], International Linear Collider (ILC) [**?** ], high-energy LHC (HE-LHC), future circular *pp* colliders of the European initiative, FCC-hh [**?** ] and the Chinese initiative, SppC [**?** ] will require high precision measurements of particle and jets at large transverse momenta. The usage of timing information for such experiments can provide additional information that can be used to improve particle and jet reconstruction, as well as to deal with background events. At this

*Email addresses:* a9510130375@gmail.com (C.-H. Yeh), chekanov@anl.gov (S.V. Chekanov), ashutosh.kotwal@duke.edu (A.V. Kotwal), ntran@fnal.gov (N.V. Tran), syu@cern.ch (S.-S. Yu)

moment, conceptional design reports for these experiments did not fully explore the benefits of the time of flight (TOF) measurements with tens-of-picosecond resolutions.

## 2. Proposal

A generic design of hadronic (electromagnetic) calorimeters for future particle collision experiments (HE-LHC, FCC, CLIC, ILC etc.) is based on two main characteristics: (1) high-granularity calorimeters with cells ranged from $3 \times 3$ mm$^2$ (for ECAL) to $5 \times 5$ cm$^2$ (for HCAL) in sizes. (2) timing with nanosecond precision that improves background rejection, vertex association, and detection of new particles. According to the CPAD report [**?** ], a development of picosecond time resolution for future calorimeters is one of the critical needs. Presently. high-granularity calorimeters (with ¿1 millions channels) with tens of picoseconds resolution represent a significant challenge due the large cost.

As a part of the HL-LHC upgrade program, CMS and ATLAS experiments are designing high-precision timing detectors with the time resolution of about 30 ps. They are based on silicon sensors that add an extra "dimension to event reconstruction. Such timing capabilities are not fully explored for future detectors beyond the HL-LHC upgrade. High-precision timing will be beneficial for new physics searches and b-tagging for all post-LHC experiments. For CLIC and FCC, high-precision time stamping will be essential for background rejection and pile-up mitigation.

Currently, the baseline designs of the high-granularity ECAL and HCAL of the CLIC/FCC detectors have not been optimized for precision timing in the range of a few tens of picoseconds. The latter is considered as an expensive option for many mullions of channels of these high-granularity detectors. This opens an opportunity to investigate a cost-effective timing layer (with the time resolution of smaller than 30 ps) for the post-LHC detectors. This layer will be installed on front of high-granularity calorimeters, covering both the forward and barrel regions.

In this paper we will investigate physics advantages for timing layers in the front of calorimeters of the post-LHC experiments. Typically, thin detectors on front of calorimeters are called "preshower". The design goal of such detectors is to count the number of charged particles in oder to correct for energy loses. The timing information of "mips" ( minimumionising particles) is not used for particle identifications. Unlike the standard pre-shower detector, we propose not only count mips, but also reconstruct high-precision timing and the position. This timing detector will have a similar granularity as the proposed high-granularity EM calorimeters themselves, but will have a sensor technology and readout which is best suited for mip time stamping (not necessarily for energy reconstruction). Our proposal is to enclose the EM detectors with two timing layers, one - before the first EM layer, and the second is after the last EM layer (but before the HCAL). The two layers of the timing detector allows a robust identification of time by correlating the position and timestamps of the particle passing through the ECAL.

In this paper we will explore this idea using full Monte Carlo simulations. A schematic representation of the positions of the timing layers for a generic detector geometry is shown in Fig. 1

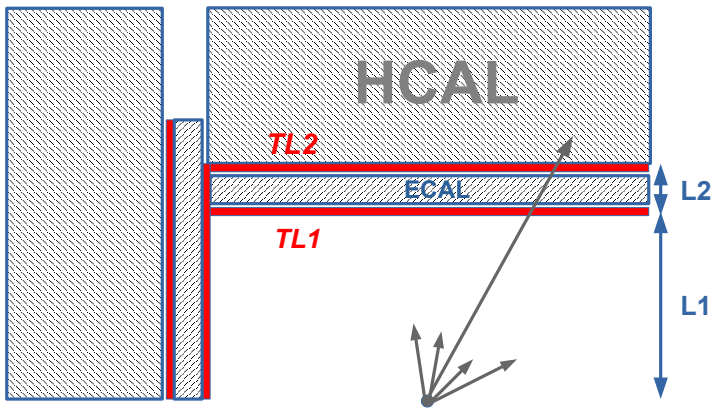


Figure 1: An example of positions of the thin timing layers for a generic detector. The thin timing layers will enclose the electromagnetic calorimeter, allow a reliable reconstruction of the mip signals with a timing resolution of the order of 10 ps.

The second layer of the timing detector can be justified if fluctuations of hits times are smaller than the resolution of the timing layers. In oder to verify this, we used a full Geant4 (version 10.3) [**?** ] simulation of the SiFCC detector [**?** ] that allows to use the information on hits from the ECAL. The ECAL is built from a highly segmented silicon-tungsten with the transverse cell size of $2 \times 2$ cm. The ECAL has 30 layers built from tungsten pads with silicon readout, corresponding to 35 $X_0$. The first 20 layers use tungsten of 3 mm thickness. The last ten layers use tungsten layers of twice the thickness, and thus have half the sampling fraction.

To verify that the time differences between last and first layer of ECAL is sufficiently small, and can be neglected for the timing layers that have a timing resolution of the order of 10 ns, a sample of single pions was created with 1 and 10 GeV momenta. The particles were reconstructed in the ECAL calorimeter, and the time difference $\Delta T = T_{\text{last}} - T_{\text{first}}$ of the hits between the last and first ECAL layers was calculated. Only hits that arrive first were considered. Figure 2 shows the time distribution for 1 and 10 GeV pions. It can be seen that the peak positions of the distributions are smaller than 1 ps, as expected for the distance of about 20 cm between the last and first layers[1]. More importantly, the RMS of these distributions are significantly smaller than the 10 ns. Therefore, for the timing layers that have a resolution of the order of 10-20 ns, a single particle crossing the two layers will be seen a single simultaneous hit, thus such hits can be well correlated in time and identified as a single crossing particle.

[1]The precision with which the simulations were performed are about 0.2-0.3 ns

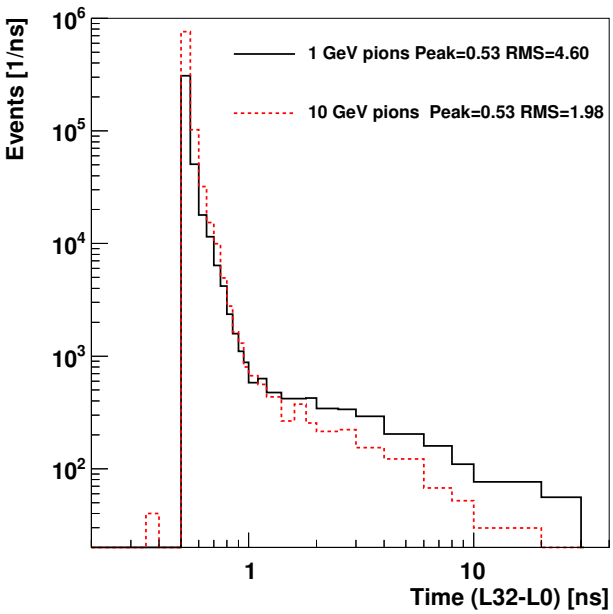


Figure 2: The difference between time of hits between the last and first layer of ECAL for single pions with the transverse momentum 1 and 10 GeV. Only first (fastest) hits were considered

## 3. Timing layers for single particles

Before considering the full Geant4 simulation, let us discuss the benefit of the TOF information for identification of separate particles. Fig. 3 shows the $3\sigma$ separation from the pion mass hypothesis using the same procedure as discussed in [**?** ]. The calculations are performed for several options for the resolution of the timing layer, from 10 ps to 1 ns, as a function of the travel length $L$ and the momenta. For a 20 ps detector and for a typical travel distance of $L \sim 0.2$ m from the interaction point to the electromagnetic calorimeter, neutrons (and protons) can be separated from the pion hypothesis up to 7 GeV. The separation of $K-$mesons can be performed up to 3 GeV. This momentum range should be sufficient for reliable particle identification in a wide range of physics studies, especially if such identification is used for jets that are dominated by this momentum range of separate particles. For a detector with 1 ns, the separation can only be possible up to 300 – 500 MeV. This is below than a typical minimum transverse momentum of 0.5 – 1 GeV for particles considered for high-energy proton colliders . Therefore, a timing layer with 1 ns resolution cannot effectively be used for particle identification in such experiments.

## 4. Timing layers for FCC and jets

In the previous sections, the capability of the timing among the various resolutions of the detector used on distinguishing the different kinds of single particle that has the different mass, momentum as well as the length of going through the detector is well-investigated as the excellent variable within the three sigma hypothesis. The next necessary step is to employ the timing, which is the potential method of discriminating the different number of the subjets within a large radius jet as well, into tackling the intractable dilemma that has been being concerned about on the highly-boosted circumstances resulting in the particles of the jet are too close to each other, and the truth number of the subjet could be misestimated, along with impacting on the analysis in the future dramatically.

The simplified-cases simulating the pileup-free conditions with the already-known processes are involved in these studies under the environment of a very-high-energy collider will be explored as the benchmark of the timing applied in the future. The same processes of Z'→qq(Background), Z'→WW(Signal) with 5, 10, 20 and 40TeV center-of-mass energy(C.M.) as the ones exploited in our second paper, are taken into account as the targets of doing the researches on the same matter with the timing implemented.

In terms of digging out the potential of the timing, several studies have been done trying on a couple of variables to see whether the timing can give us another degree of information helping on having the improvement on the issue in addition to the $P_T$ that we could obtain directly from the detector . The $\Delta R$, which is the common variable that has been being used in the collider as acquiring the angle between two particles/-jets, is found to be the possible one that can take advantage of using the timing to analyze the structure of the jets more evidently. Also, the ideal cases of separating the different particles with the help of the timing are also premeditated.

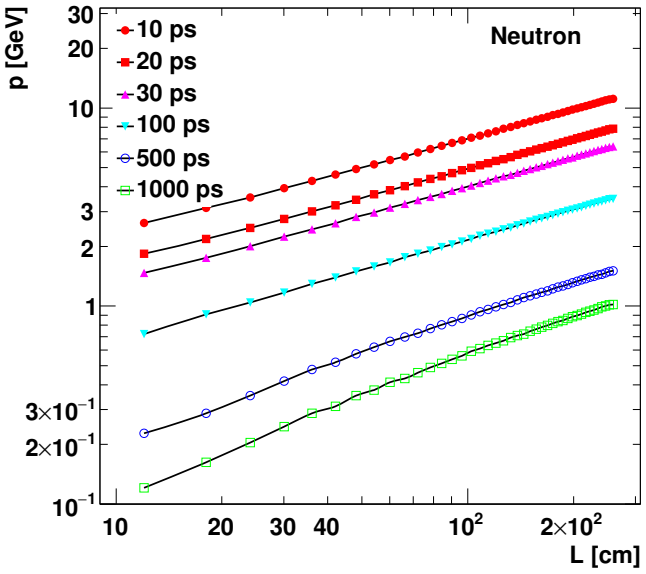


(a) Neutrons

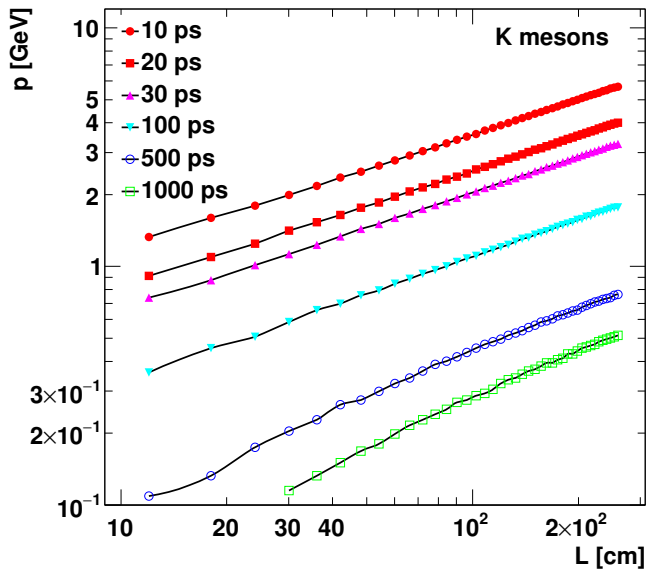


(b) $K$-mesons

Figure 3: The $3\sigma$ separation from the pion mass for neutrons and $K$-mesons as a function of the distance and the momenta.

The two sets of the collections of the data including both of the generator level(truth-level) and the reconstruction level(reco-level) are utilized in the studies for the purpose of corresponding between each other as the benchmark of the parameters that are found beneficial. At the first place, the definition of many terms applied in the studies will be well-defined as a favor of proceeding smoothly. The second one is to make use of the truth-level information of the four momenta for each particle to figure out the anticipation of the timing being capable of helping on the issue at best ideally. Last but not least, the well-established cases illustrated by using the reco-level information of the non-smearing four momenta and the fastest-response timing[2] from each cell of the calorimeter will be given as the true cases we could expect in our life when the time of the timing-capable detector installed in the collider with the very high C.M. energy comes.

### *4.1. The definitions of the terms introduced in the following studies*

In case for avoiding being confused by the terms applied in these studies, predefining for those terms is essential.

#### *4.1.1. The timing used in the truth-level cases*

At the first place, the definition of the timing should be obtained as our benchmark to do these studies when dealing with the truth-level information. The standard formula of the timing is as follows for each particle:

$$Timing = \frac{L(\eta)}{V(V_x, V_y, V_z)} \tag{1}$$

Basically, it is the normal formula of the time of flight(TOF), depending on the different $\eta$, leading to the different distances $L$ between collision point and HCAL barrel, along with the three-dimensional velocities $V$ of the particles.

But, since the effect of the magnetic field is taken into account, the timing applied in this paper is the modified one with only considering the Z direction of the distance and velocity, and then we can get more precise value of the timing by the truth of the Z-direction trace of the particle isn't changed by the magnetic field. The formula used in this paper is as follows:

$$Timing = \frac{L_z}{V(V_z)} \tag{2}$$

After applying this formula on all particles, and the timing can be obtained without the bending effect coming from the magnetic field.

[2] As a matter of fact that the detector can response to the first-arrival particle barely in one event, the timing observed from the reco-level can merely be treated as the part of the jet but not the whole one. Oppositely, the particles of the four momenta from a jet can be explicitly known from the information of the truth-level, and the timing of each particle should be well-calculated with the formula of the timing listed in the following sections as the ideal cases.

*4.1.2. The trailing particles applied in all cases*

The another terms should be noticed as the important ones are two sorts of the trailing particles applied in all cases. The definition of the trailing particles defined by the Timing(T) and transverse momentum(PT) should be clarified. We have two categories of the trailing particles

1. Defined by the T, so-called "trailing-T", meaning that the particle has the longest traveling timing in the jet.
2. Defined by the PT, so-called "trailing-$P_T$", meaning that the lowest-PT particle in the jet.

Subsequently, we can define the next-to trailing particle as well, such as the second long traveling timing-"next-to-trailing-T"(The second trailing-T) or the second low PT-"next-to-trailing-$P_T$"(The second trailing-$P_T$), and so on. The order of the trailing particle will be well-specified in the following section.

*4.2. The truth-level studies*

In order to compare the studies carried out by the truth-level information with the ones done at the reco-level, the selection of the events at the generator level should be enlightened at first. At the first place, since the information of the four momenta upon the particles reconstructed by HCAL barrel in SiFCC will be utilized as the candidates of excavating the potential of the timing, the pre-selection of the eta on the particles should be aligned with the HCAL which is in the region of $1 < |\eta| < 2$. Subsequently, the effect of the magnetic field should be concerned as the probably authentic situation occurring in the collider. With the calculations played out by $P_T = 0.3RT$, the cut down limit of the energy owned by the particles is about 1.5GeV.

With the necessary selection applied on, the advantageous of the timing can be probed thoroughly with the truth-level information. In the following studies, to begin with, the studies of making up the decision on the chosen trailing particles exploited in the succeeding sections will be elaborated on, afterwards, the $\Delta R$, which is found to be the useful parameter with the chosen trailing particles, will be the next theme describing on how it can help on solving the subjet-number issue.

*4.2.1. The study of the chosen trailing particles*

So as to figure out the extra dimension that can be taken advantage of from the timing, the original dimension of $P_T$ is considered in this study as the competition to see whether the benefit of the timing can be obtained upon it.

Fig.18 to Fig.5 are two plots showing the particle identification with two kinds of trailing particles up to the fifth order. By comparing these two plots, the fascinating point is that the 10% improvement on tagging the protons can be given as employing the timing in. Since the histograms of both kinds of trailing particles after the fifth order show the similar distributions, implying the limitation of the timing upon the $P_T$ is up till there, the order up to fifth for both sorts of trailing particles will be the chosen ones in the following sections.

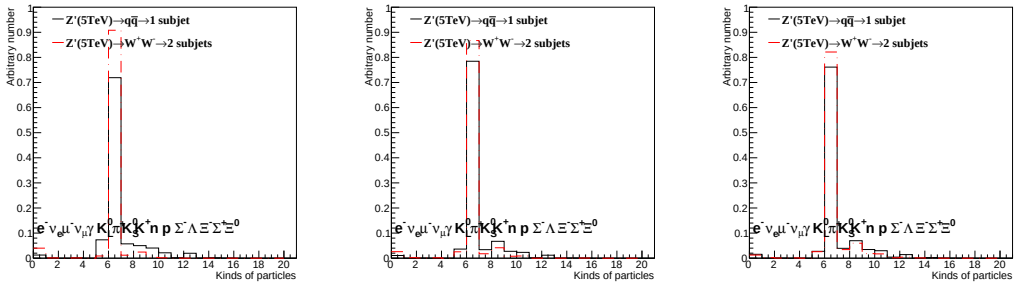


(a) The first trailing-$P_T$ (b) The second trailing-$P_T$ (c) The third trailing-$P_T$

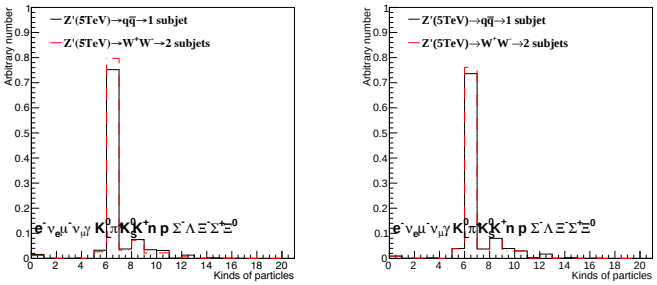


(d) The fourth trailing-$P_T$ (e) The fifth trailing-$P_T$

Figure 4: Distributions of particle ID for $M(Z') = 5$ TeV for five kinds of trailing-$P_T$ particles with the truth-level information are shown here.

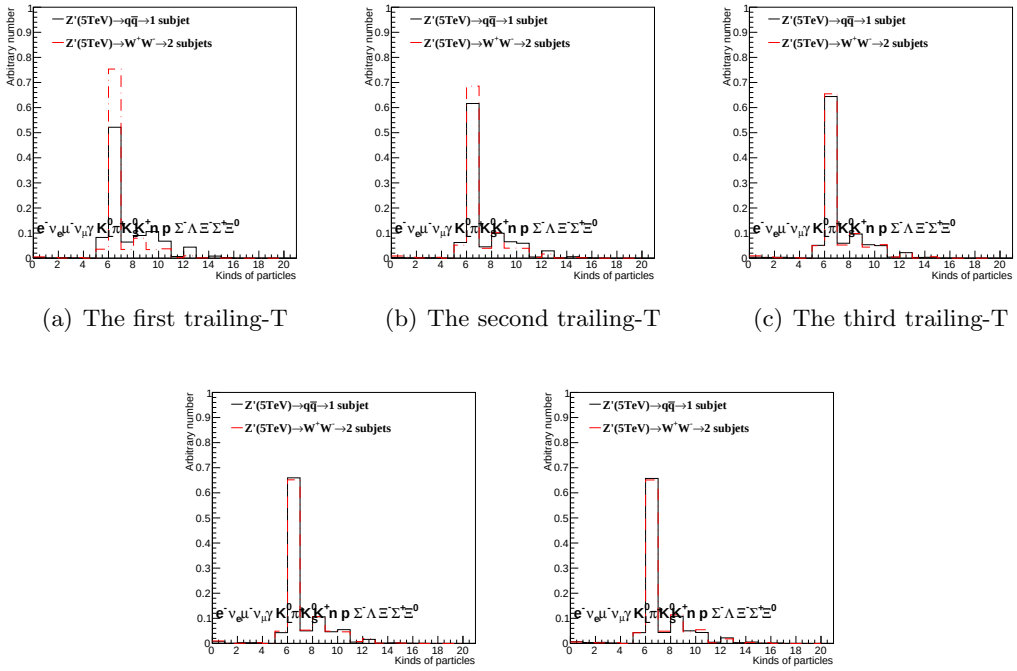


(a) The first trailing-T (b) The second trailing-T (c) The third trailing-T

(d) The fourth trailing-T (e) The fifth trailing-T

Figure 5: Distributions of particle ID for $M(Z') = 5$ TeV for five kinds of trailing-$P_T$ particles with the truth-level information are shown here.

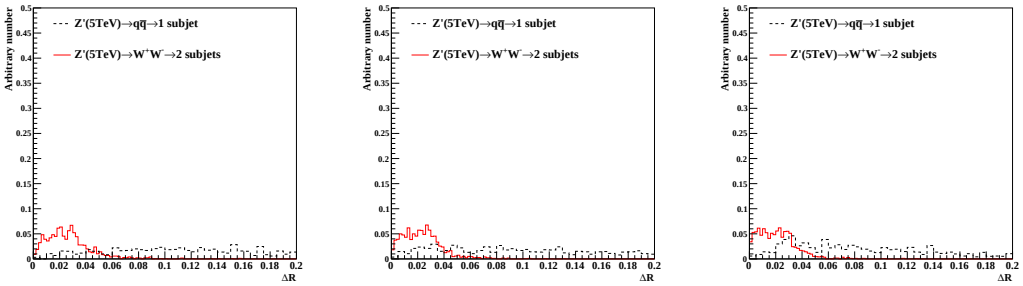


(a) The first trailing-$P_T$ (b) The second trailing-$P_T$ (c) The third trailing-$P_T$

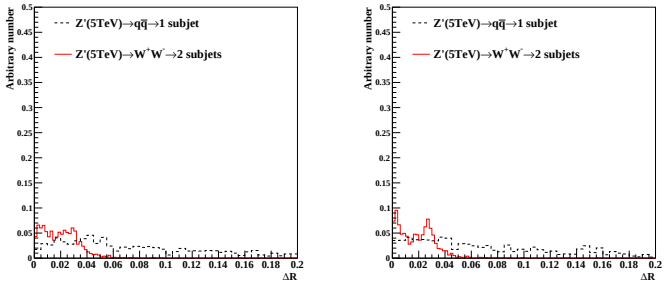


(d) The fourth trailing-$P_T$ (e) The fifth trailing-$P_T$

Figure 6: Distributions of $\Delta R$ for $M(Z') = 5$ TeV for five kinds of trailing-$P_T$ particles with the truth-level information are shown here.

### *4.2.2.* $\Delta R$

Fig.22 to Fig.9 show some of the distributions of $\Delta R$, which are the angles between the Leading-$P_T$ particle and the chosen trailing particles, demonstrated by resonance masses of 5TeV and 40TeV individually as two extreme cases explaining on the discriminations phenomenologically. The power of $\Delta R$ applied to discern the jets containing the various number of the subjets is displayed off obviously with those plots.

For the distributions of Z'→qq of both resonance masses, the mass-independent extensive shapes ranging from 0 to 0.2 can be easily recognized in all cases. Oppositely, the mass-dependent distributions of $\Delta R$ observed by the Z'→WW can be acquainted conspicuously. The lower mass case of Z'→WW at 5TeV shown in Fig 22 and Fig.7 shows the very different behavior compared with the ones acquired from 40TeV case, which is illustrated in Fig.25 and Fig 9 displaying the very narrow distributions centralizing near the 0. Those schemes can be used as a proof of $\Delta R$ is the great variable for distinguishing the different subjet cases by the large-separation appearance obtained from the higher mass case.

After performing the separation power of $\Delta R$ with the histograms qualitatively, the quantitive way with the module of the Boosted Decision Tree(BDT) will be utilized as investigating the power of the discrimination for all four resonance masses. In

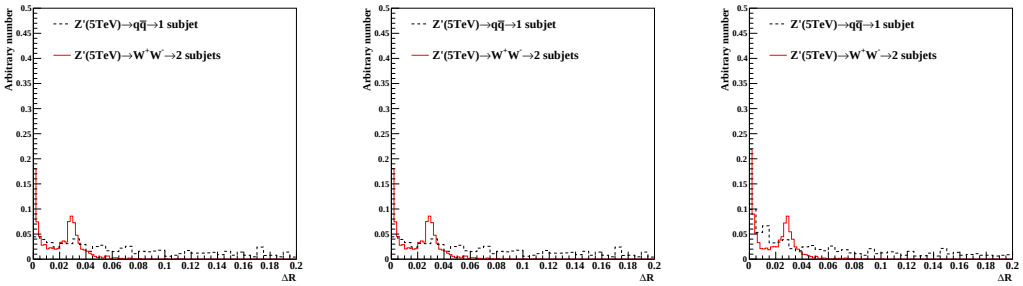


(a) The first trailing-T (b) The second trailing-T (c) The third trailing-T

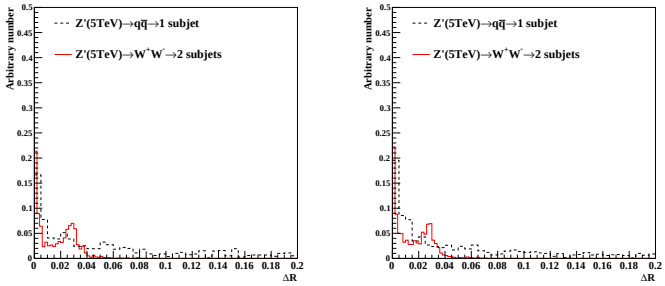


(d) The fourth trailing-T (e) The fifth trailing-T

Figure 7: Distributions of $\Delta R$ for $M(Z') = 5$ TeV for five kinds of trailing-T particles with the truth-level information are shown here.

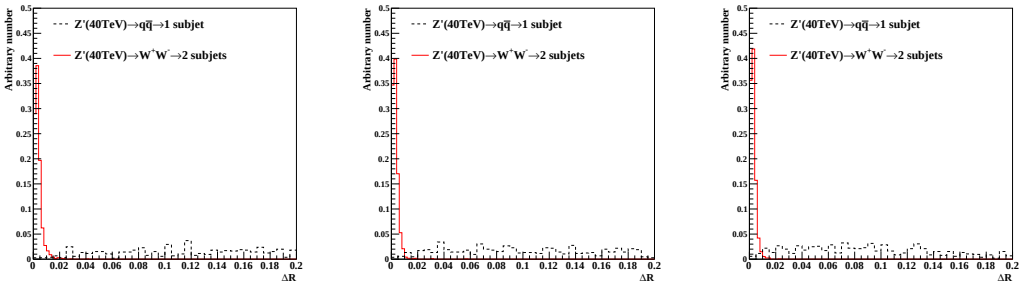


(a) The first trailing-$P_T$ (b) The second trailing-$P_T$ (c) The third trailing-$P_T$

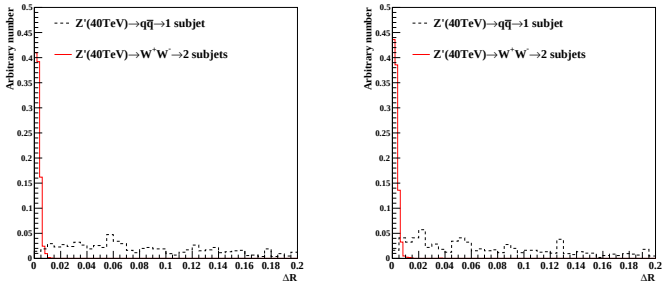


(d) The fourth trailing-$P_T$ (e) The fifth trailing-$P_T$

Figure 8: Distributions of $\Delta R$ for $M(Z') = 40$ TeV for five kinds of trailing-$P_T$ particles with the truth-level information are shown here.

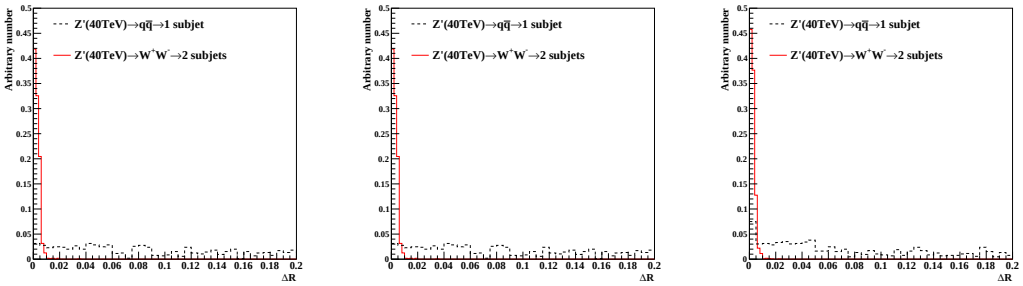


(a) The first trailing-T (b) The second trailing-T (c) The third trailing-T

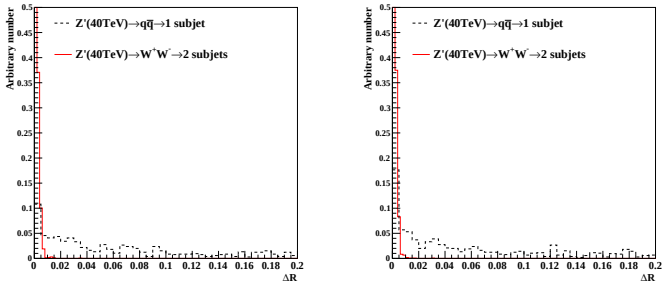


(d) The fourth trailing-T (e) The fifth trailing-$P_T$

Figure 9: Distributions of $\Delta R$ for $M(Z') = 40$ TeV for five kinds of trailing-T particles with the true information are shown here.

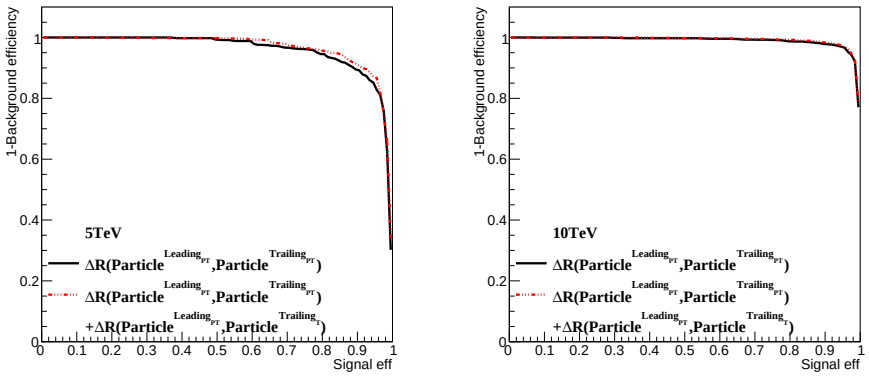


(a) 5TeV




(b) 10TeV

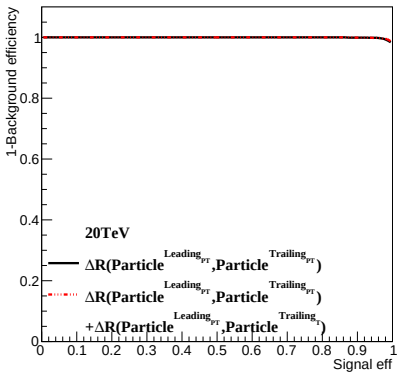


(c) 20TeV

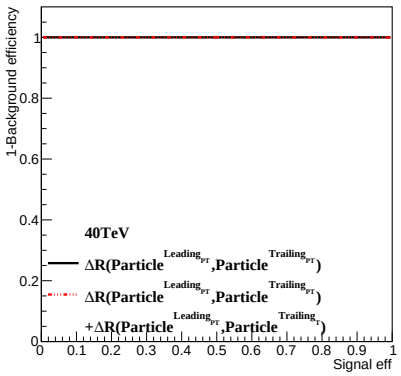


(d) 40TeV

Figure 10: The comparison of the ROC curves obtained from two cases including five trailing-$P_T$ particles up to the fifth order alone(black) and the ones accompanied by five trailing-T particles up to the fifth order(red) with the truth information of the different $M(Z')$ are shown here. The signal (background) process is $Z' \to WW$ ($Z' \to q\bar{q}$).

the Fig.10, the BDT method is applied to make out the efficiency of separating the two processes with the input variables of those chosen trailing particles for all cases. The statement which can be addressed from the plots is that the separation power of the $\Delta R$ with trailing-$P_T$ is as perfect as trailing-T, originating from the lines overlap together in the figure. In this case, the variable of $\Delta R$ is worthy for us to keep exploring on to see whether the cases are similar as the ones done with the reco-level data.

### *4.3. The reco-level studies*

Over the specific studies for the $\Delta R$ with the truth-level information in the former section, the capability of the $\Delta R$ with the timing is aware of as a a great variable as $P_T$ into investigating the different number of the subjets within a large radius jet. Followed up by that, the essential step of verifying on the efficiency of the variable applied in the real case is to prepare the reco-level data, which serves as the situations operating in the future, to corroborate the advanced of the timing employed into handling the issue.

The distributions of the $\Delta R$, which are revealed from Fig.26 to Fig.14 for 5TeV and 40TeV cases as the ones used in the truth-level studies, show that the distributions of Z'→WW and Z'→qq can't be well-separated by both trailing cases sharply at the higher C.M. point, and that is caused by the non-smearing detector resulting in the possible outcome of the $\Delta R$ can only be the value of any two-cells angle of ECAL but not the authentic angles between truth particles . Surprisingly, the timing in this case can give us a little bit improvement upon the $P_T$ cases with the proof of the BDT plots in Fig.15 summarizing the efficiency of those variables. Much improvement with the timing can be observed at the higher C.M. point.

Speaking of the $\Delta R$ which is strongly-dependent of the precise of measuring the momenta, the tracker, which can get rid of the issue on non-smearing problem happening in ECAL to explicitly measure the momentum with the high-granularity cell, is the essential detector to explore the efficiency of the parameter. The distributions of $\Delta R$ with the tracker are posted in Fig.16 and Fig.17, that show the circumstances are very similar to the truth-level ones in case the precise four momenta can be sought out, the better separation between two different number of subjets can be discovered. As the schemes of BDT plots shown in Fig.15 as the one mentioned in the previous paragraph, the line obtained from the tracker with the chosen trailing-$P_T$ particles[3] shows that the high-rejection of the background with the accurate measurement of the four momenta can be used as the mean completing the task of distinguishing the different number of subjet.

[3]At the moment, since the timing information from the tracker in our current simulation can't be acquired as another detectors, we only apply the trailing-$P_T$ for the tracker case.

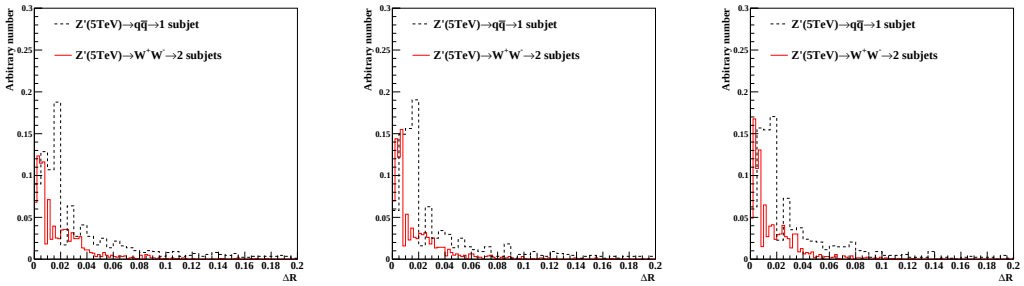


(a) The first trailing-PT (b) The second trailing-T (c) The third trailing-T

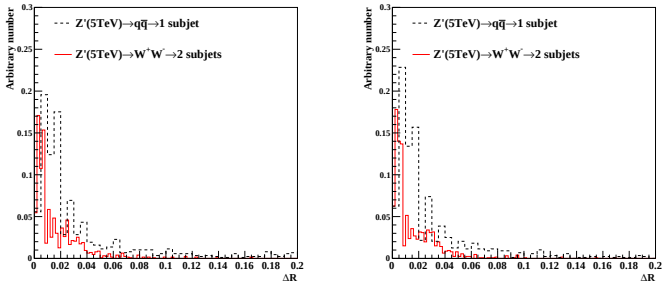


(d) The fourth trailing-T (e) The fifth trailing-T

Figure 11: Distributions of $\Delta R$ for $M(Z') = 5$ TeV for five kinds of trailing-$P_T$ particles with the reco-level information of ECAL are shown here.

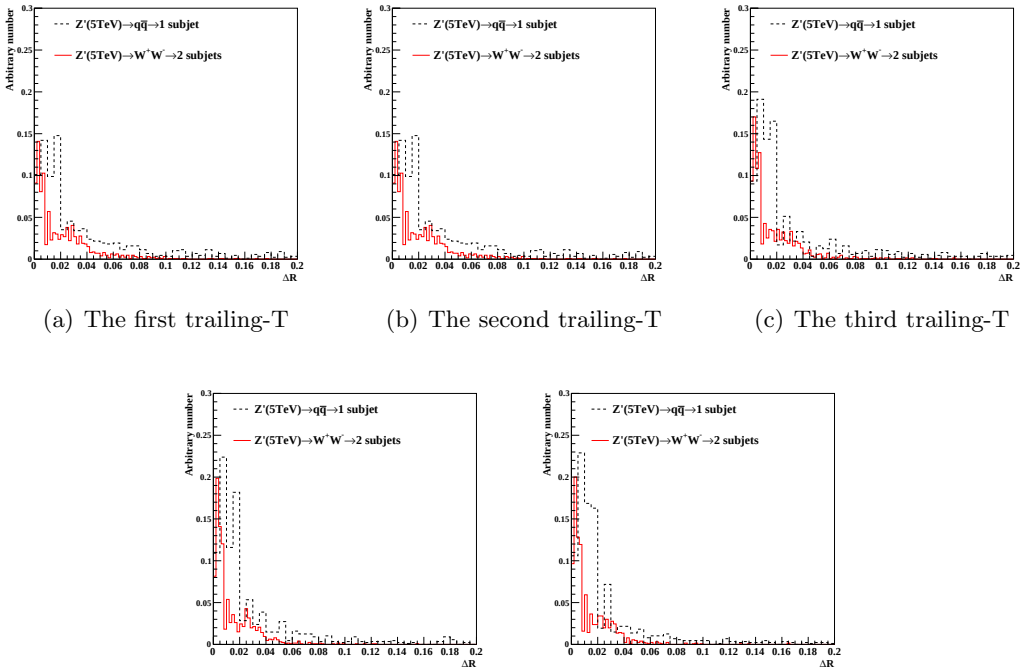


(a) The first trailing-T (b) The second trailing-T (c) The third trailing-T

(d) The fourth trailing-T (e) The fifth trailing-T

Figure 12: Distributions of $\Delta R$ for $M(Z') = 5$ TeV for five kinds of trailing-T particles with the reco-level information of ECAL are shown here.

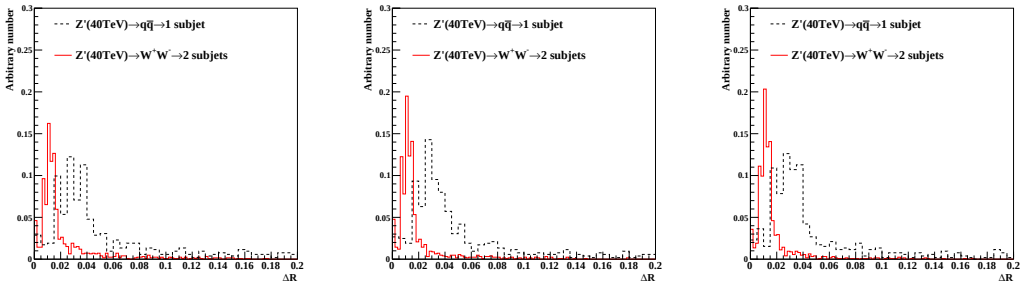


(a) The first trailing-PT (b) The second trailing-PT (c) The third trailing-PT

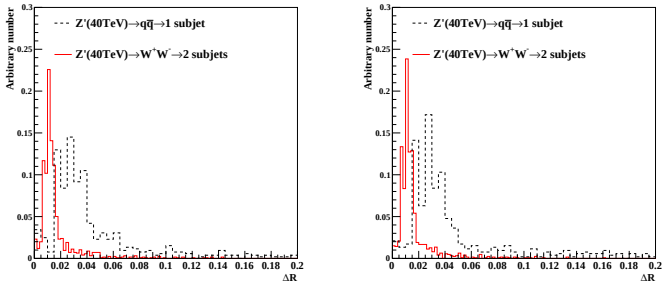


(d) The fourth trailing-PT (e) The fifth trailing-PT

Figure 13: Distributions of $\Delta R$ for $M(Z') = 40$ TeV for five kinds of trailing-$P_T$ particles with the reco-level information of ECAL are shown here.

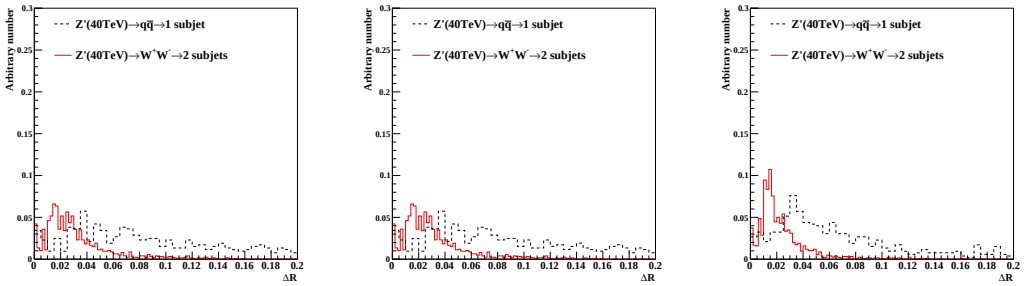


(a) The first trailing-T (b) The second trailing-T (c) The third trailing-T

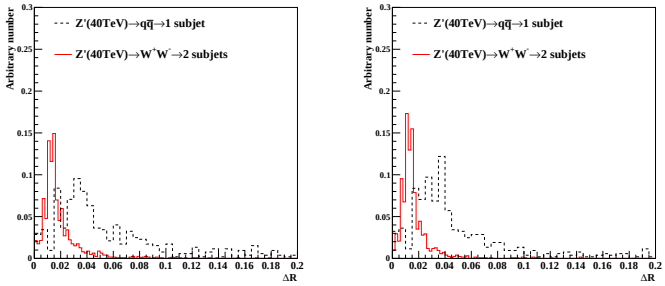


(d) The fourth trailing-T (e) The fifth trailing-T

Figure 14: Distributions of $\Delta R$ for $M(Z') = 40$ TeV for five kinds of trailing-T particles with the reco-level information of ECAL are shown here.

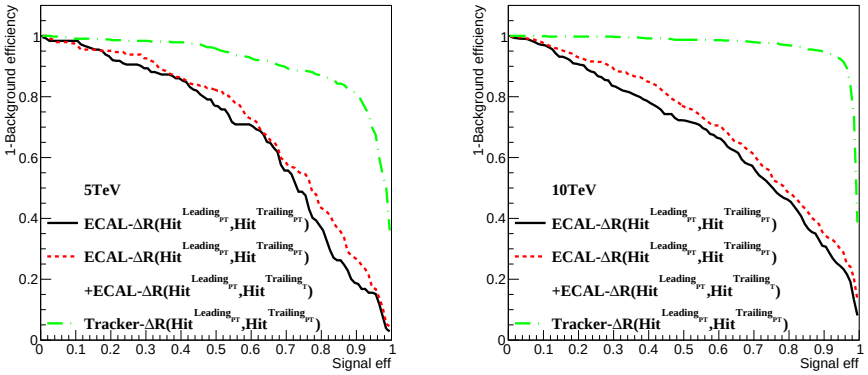


(a) 5TeV (b) 10TeV

(c) 20TeV (d) 40TeV

Figure 15: The comparison of the ROC curves obtained from two cases including five trailing-$P_T$ particles of ECAL up to the fifth order alone(black) and the ones accompanied by five trailing-T particles of ECAL up to the same order(red), as well we the one drawn with trailing-$P_T$ particles of the tracker up to the same order(green) with the reco-level information of the different $M(Z')$ are shown here. The signal (background) process is $Z' \to WW$ ($Z' \to q\bar{q}$).

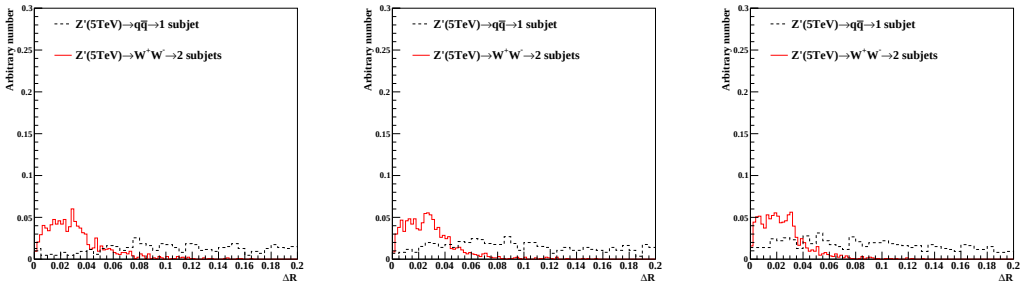


(a) The first trailing-T (b) The second trailing-T (c) The third trailing-T

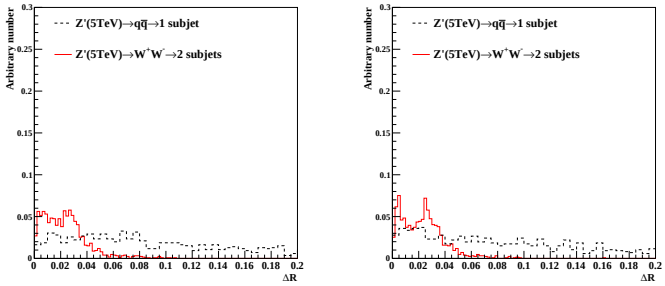


(d) The fourth trailing-T (e) The fifth trailing-T

Figure 16: Distributions of $\Delta R$ for $M(Z') = 5$ TeV for five kinds of trailing-$P_T$ particles with the reco-level information of tracker are shown here.

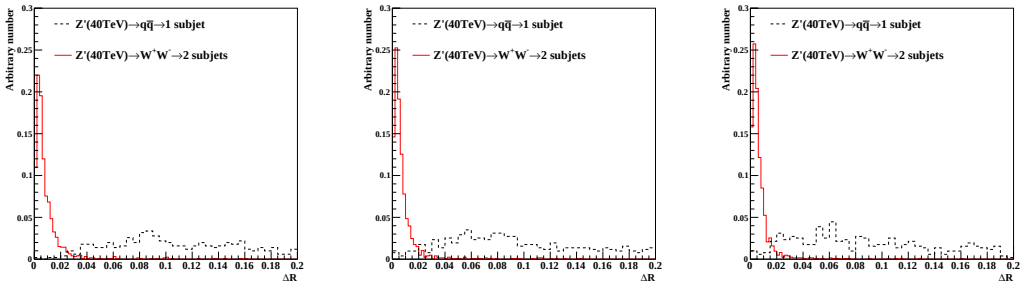


(a) The first trailing-T (b) The second trailing-T (c) The third trailing-T

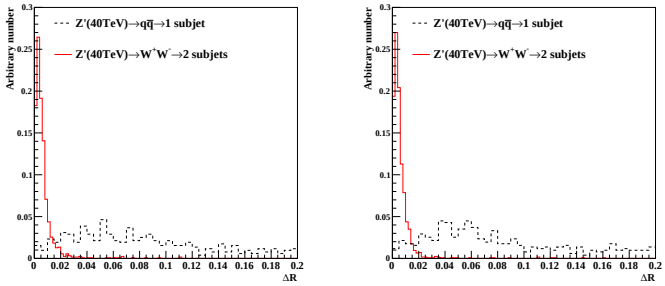


(d) The fourth trailing-T (e) The fifth trailing-T

Figure 17: Distributions of $\Delta R$ for $M(Z') = 40$ TeV for five kinds of trailing-$P_T$ particles with the reco-level information of tracker are shown here.

**5. Pick up the histograms**

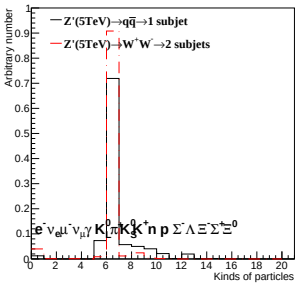


(a) The first trailing-$P_T$

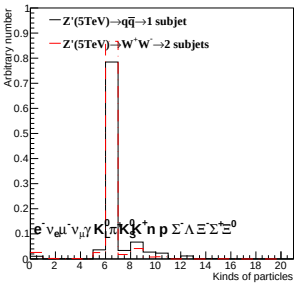


(b) The second trailing-$P_T$

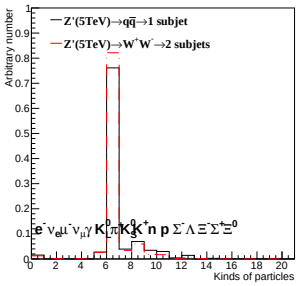


(c) The third trailing-$P_T$

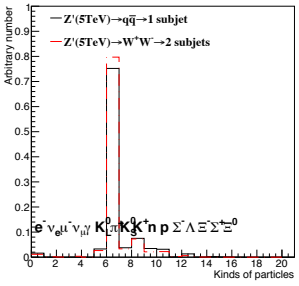


(d) The fourth trailing-$P_T$

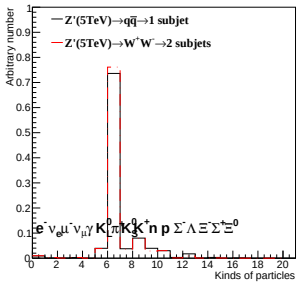


(e) The fifth trailing-$P_T$

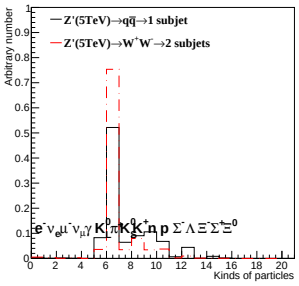


(f) The first trailing-T

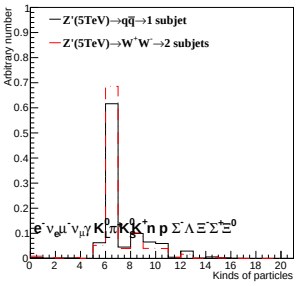


(g) The second trailing-T

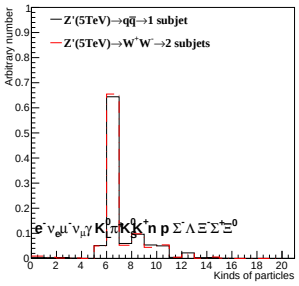


(h) The third trailing-T

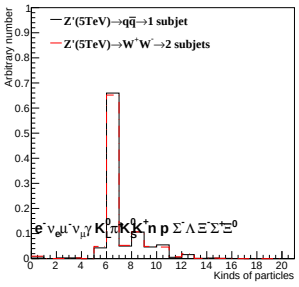


(i) The fourth trailing-T

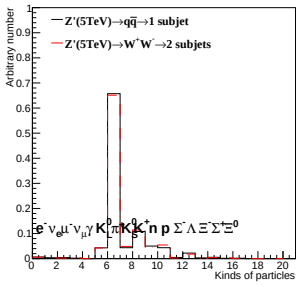


(j) The fifth trailing-T

Figure 18: Distributions of particle ID for $M(Z') = 5$ TeV for five kinds of trailing particles with the truth-level information are shown here.

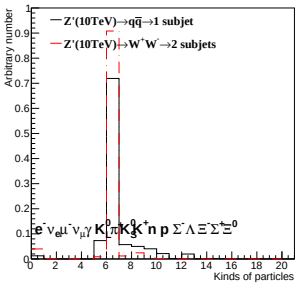


(a) The first trailing-$P_T$

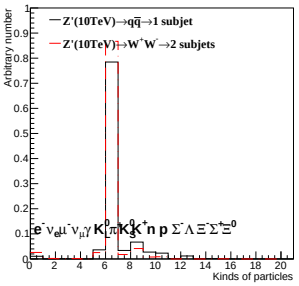


(b) The second trailing-$P_T$

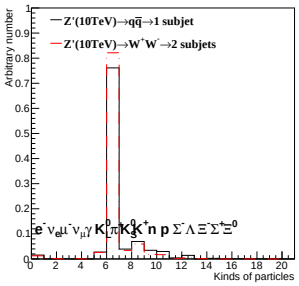


(c) The third trailing-$P_T$

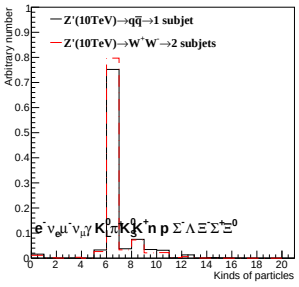


(d) The fourth trailing-$P_T$

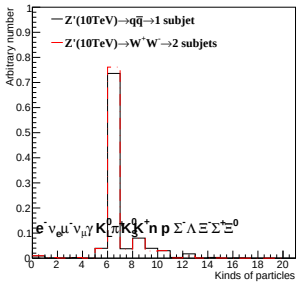


(e) The fifth trailing-$P_T$

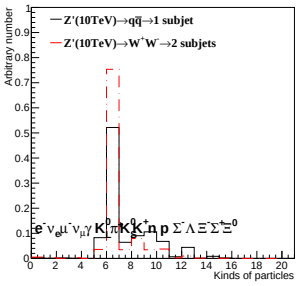


(f) The first trailing-T

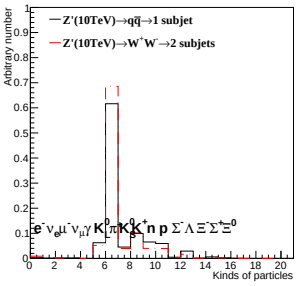


(g) The second trailing-T

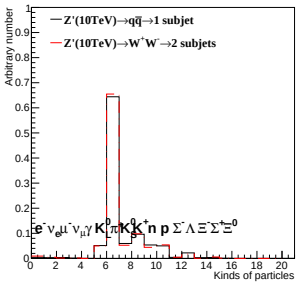


(h) The third trailing-T

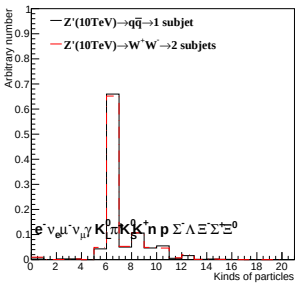


(i) The fourth trailing-T

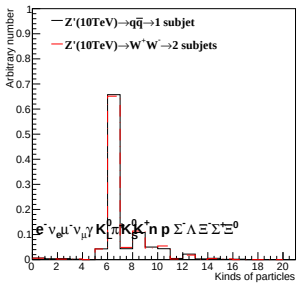


(j) The fifth trailing-T

Figure 19: Distributions of particle ID for $M(Z') = 10$ TeV for five kinds of trailing particles with the truth-level information are shown here.

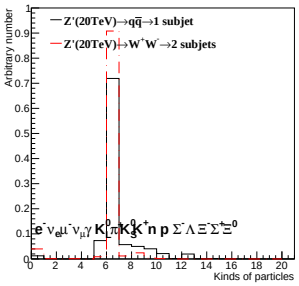


(a) The first trailing-$P_T$

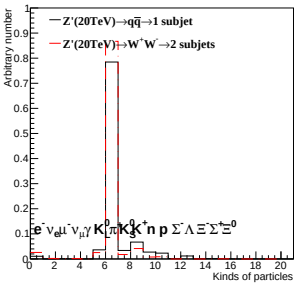


(b) The second trailing-$P_T$

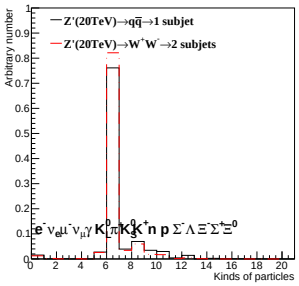


(c) The third trailing-$P_T$

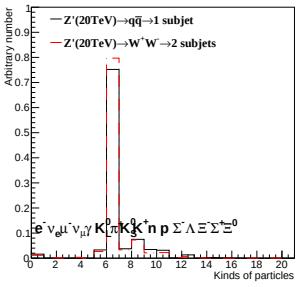


(d) The fourth trailing-$P_T$

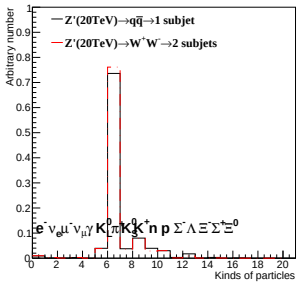


(e) The fifth trailing-$P_T$

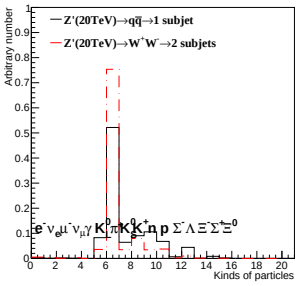


(f) The first trailing-T

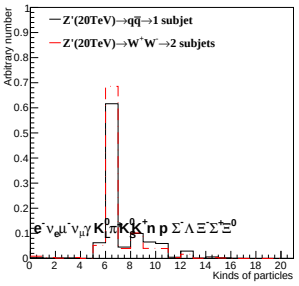


(g) The second trailing-T

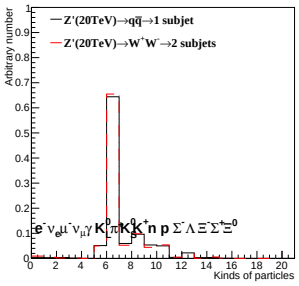


(h) The third trailing-T

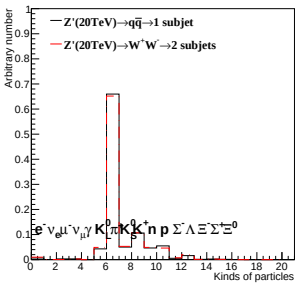


(i) The fourth trailing-T

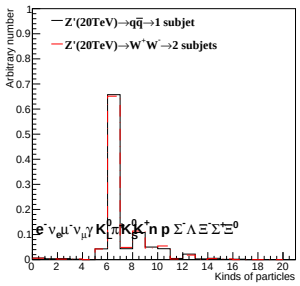


(j) The fifth trailing-T

Figure 20: Distributions of particle ID for $M(Z') = 20$ TeV for five kinds of trailing particles with the truth-level information are shown here.

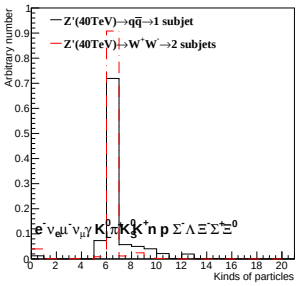


(a) The first trailing-$P_T$

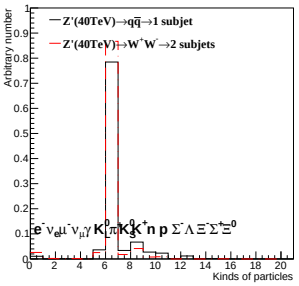


(b) The second trailing-$P_T$

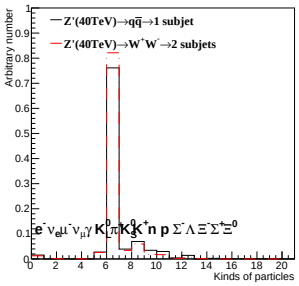


(c) The third trailing-$P_T$

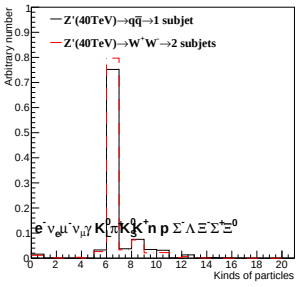


(d) The fourth trailing-$P_T$

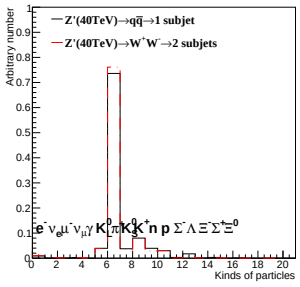


(e) The fifth trailing-$P_T$

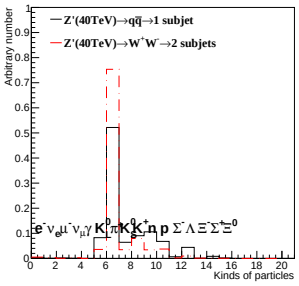


(f) The first trailing-T

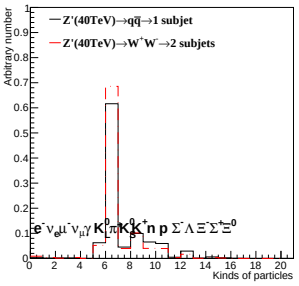


(g) The second trailing-T

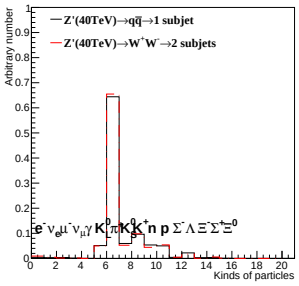


(h) The third trailing-T

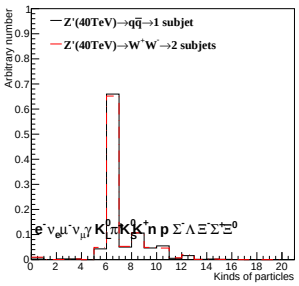


(i) The fourth trailing-T

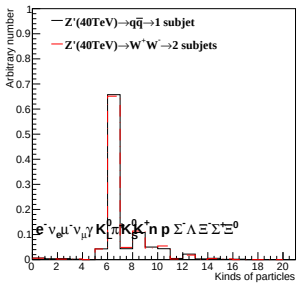


(j) The fifth trailing-T

Figure 21: Distributions of particle ID for $M(Z') = 40$ TeV for five kinds of trailing particles with the truth-level information are shown here.

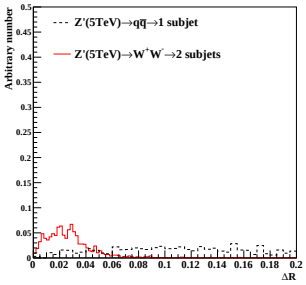


(a) The first trailing-PT

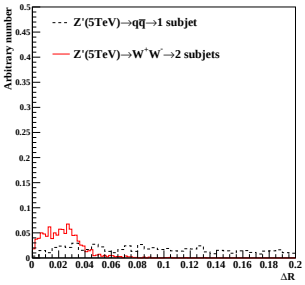


(b) The second trailing-PT

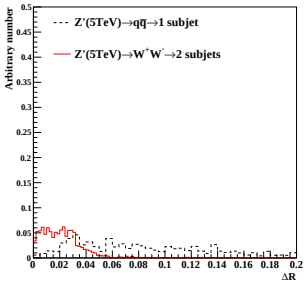


(c) The third trailing-PT

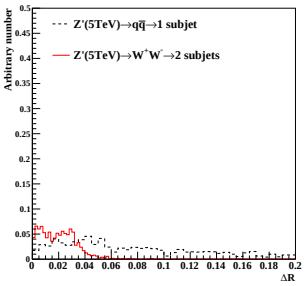


(d) The fourth trailing-PT

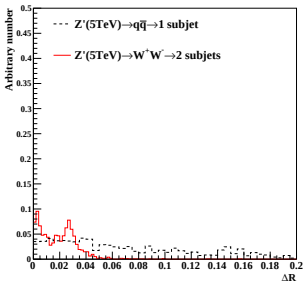


(e) The fifth trailing-PT

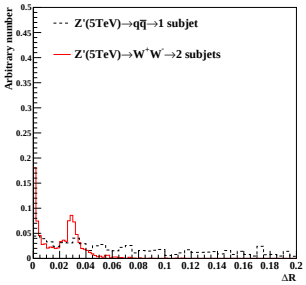


(f) The first trailing-T

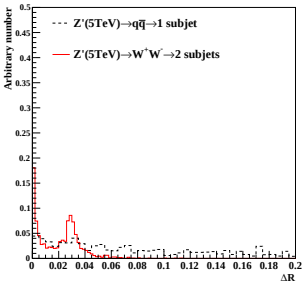


(g) The second trailing-T

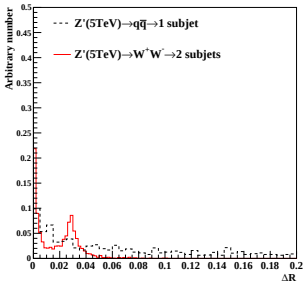


(h) The third trailing-T

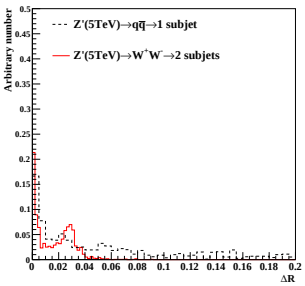


(i) The fourth trailing-T

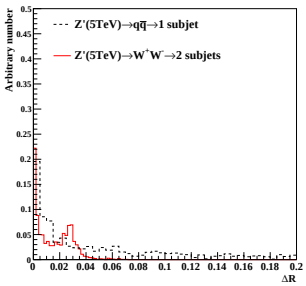


(j) The fifth trailing-T

Figure 22: Distributions of $\Delta R$ for $M(Z') = 5$ TeV for five kinds of trailing particles with the truth-level information are shown here.

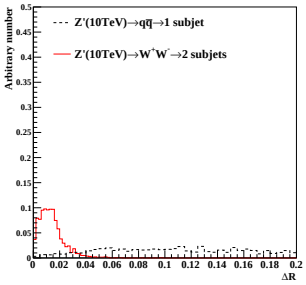


(a) The first trailing-PT

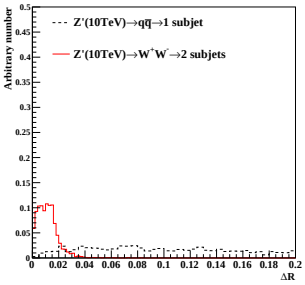


(b) The second trailing-PT

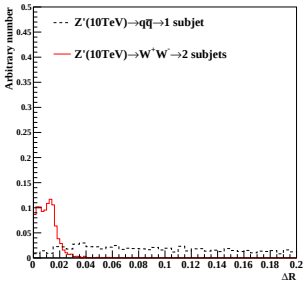


(c) The third trailing-PT

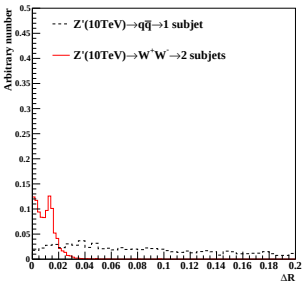


(d) The fourth trailing-PT

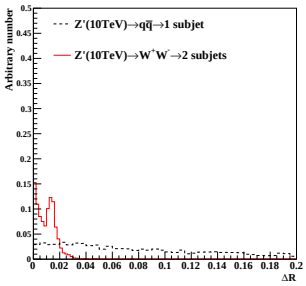


(e) The fifth trailing-PT

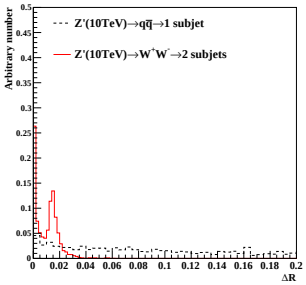


(f) The first trailing-T

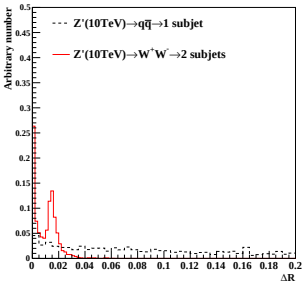


(g) The second trailing-T

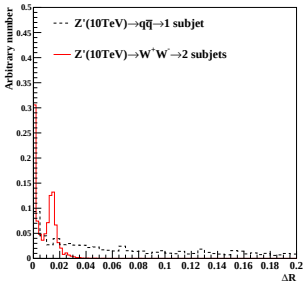


(h) The third trailing-T

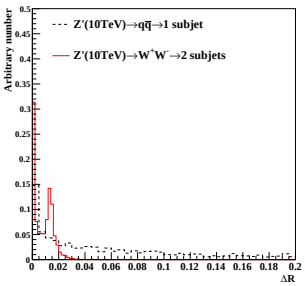


(i) The fourth trailing-T

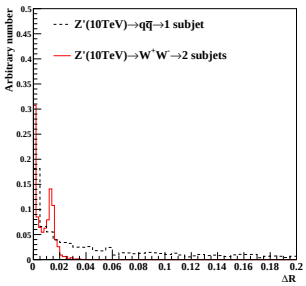


(j) The fifth trailing-T

Figure 23: Distributions of $\Delta R$ for $M(Z') = 10$ TeV for five kinds of trailing particles with the truth-level information are shown here.

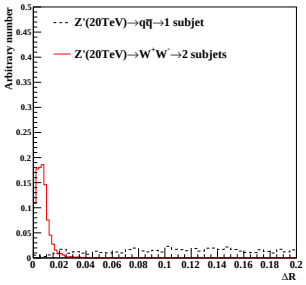


(a) The first trailing-PT

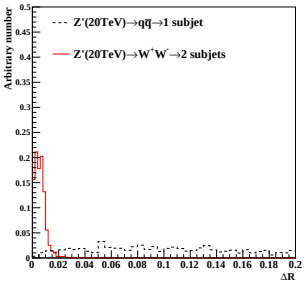


(b) The second trailing-PT

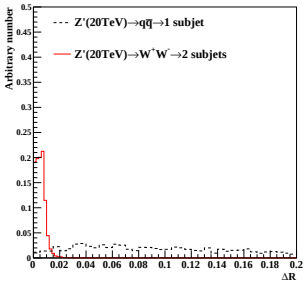


(c) The third trailing-PT

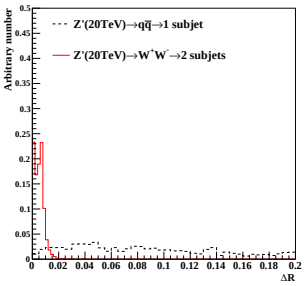


(d) The fourth trailing-PT

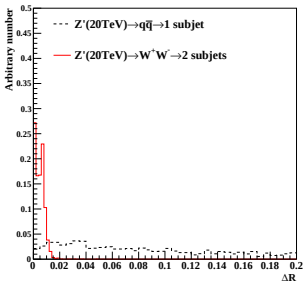


(e) The fifth trailing-PT

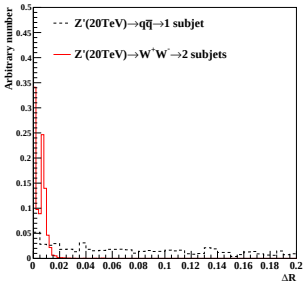


(f) The first trailing-T

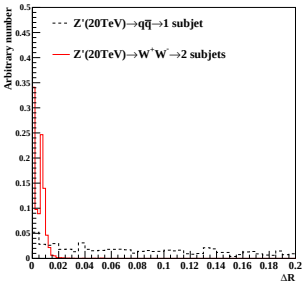


(g) The second trailing-T

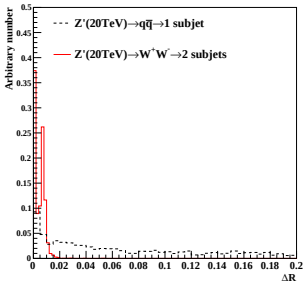


(h) The third trailing-T

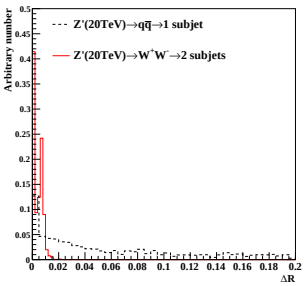


(i) The fourth trailing-T

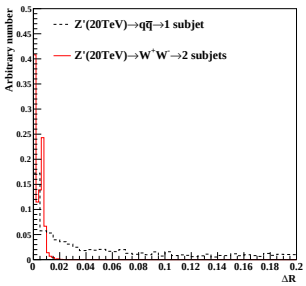


(j) The fifth trailing-T

Figure 24: Distributions of $\Delta R$ for $M(Z') = 20$ TeV for five kinds of trailing particles with the truth-level information are shown here.

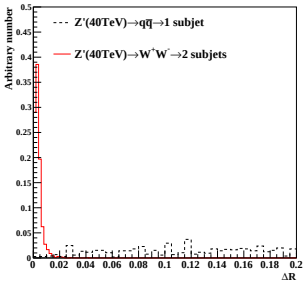


(a) The first trailing-PT

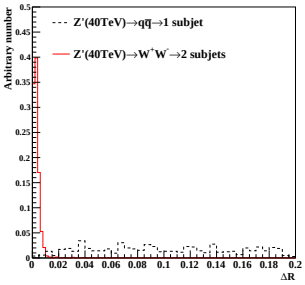


(b) The second trailing-PT

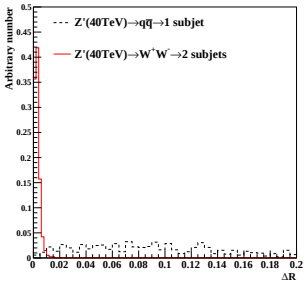


(c) The third trailing-PT

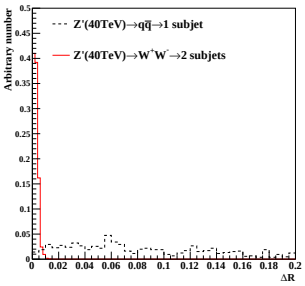


(d) The fourth trailing-PT

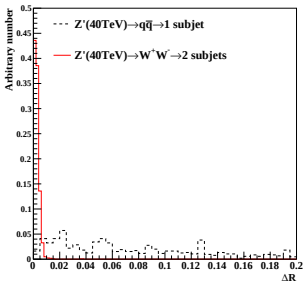


(e) The fifth trailing-PT

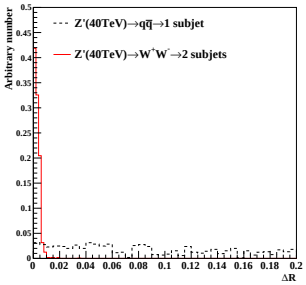


(f) The first trailing-T

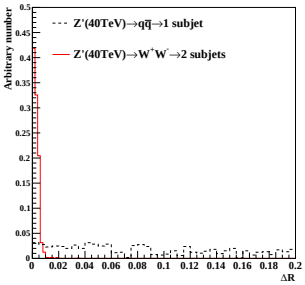


(g) The second trailing-T

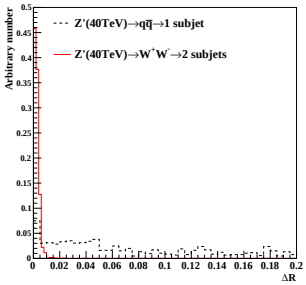


(h) The third trailing-T

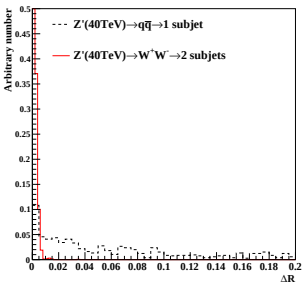


(i) The fourth trailing-T

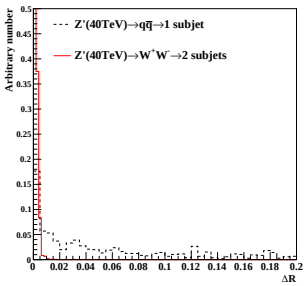


(j) The fifth trailing-T

Figure 25: Distributions of $\Delta R$ for $M(Z') = 40$ TeV for five kinds of trailing particles with the truth-level information are shown here.

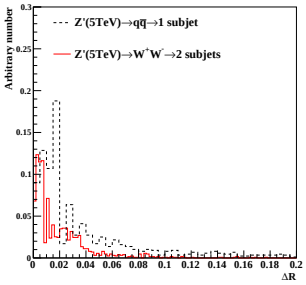


(a) The first trailing-PT

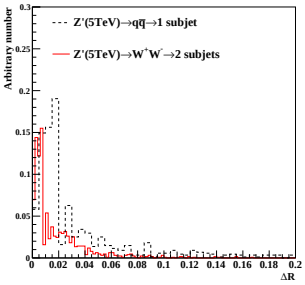


(b) The second trailing-PT

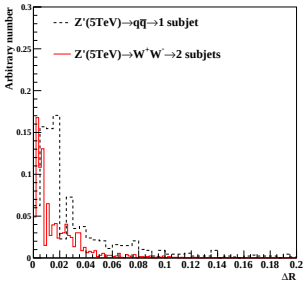


(c) The third trailing-PT

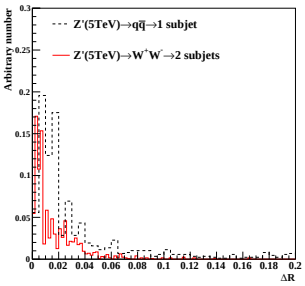


(d) The fourth trailing-PT

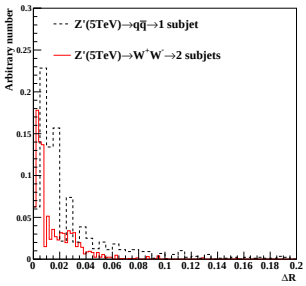


(e) The fifth trailing-PT

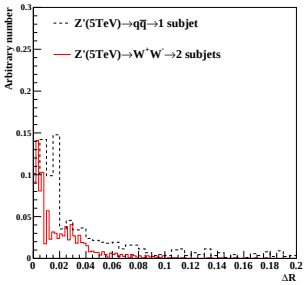


(f) The first trailing-T

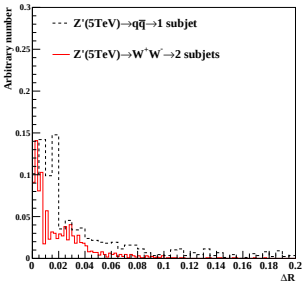


(g) The second trailing-T

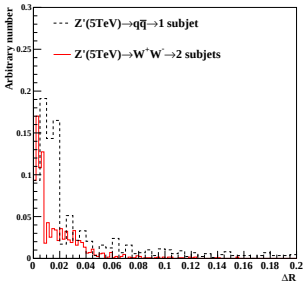


(h) The third trailing-T

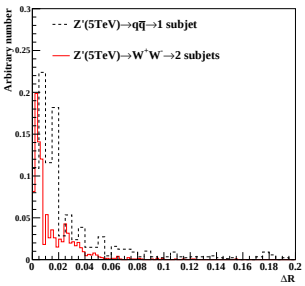


(i) The fourth trailing-T

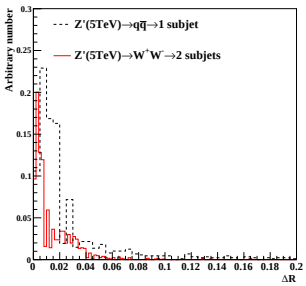


(j) The fifth trailing-T

Figure 26: Distributions of $\Delta R$ for $M(Z') = 5$ TeV for five kinds of trailing- particles with the reco-level information of ECAL are shown here.

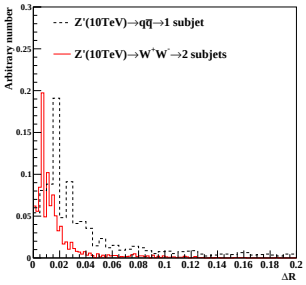


(a) The first trailing-PT

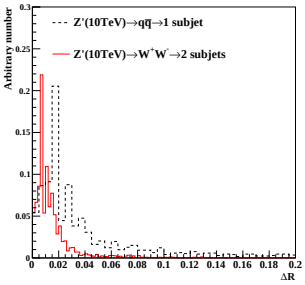


(b) The second trailing-PT

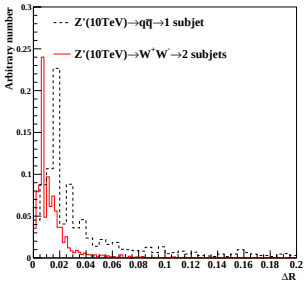


(c) The third trailing-PT

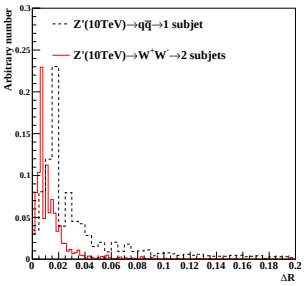


(d) The fourth trailing-PT

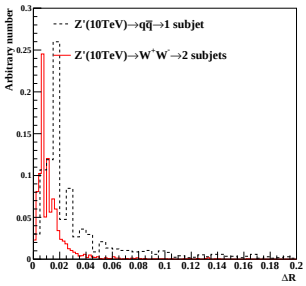


(e) The fifth trailing-PT

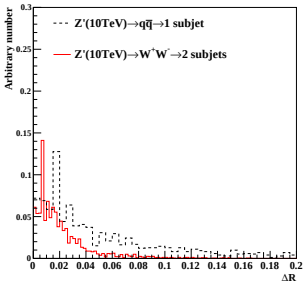


(f) The first trailing-T

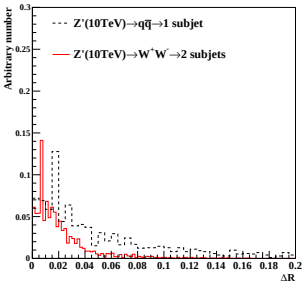


(g) The second trailing-T

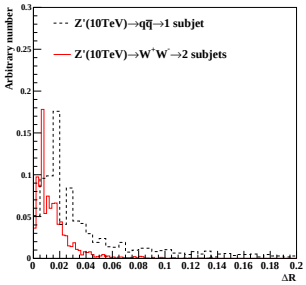


(h) The third trailing-T

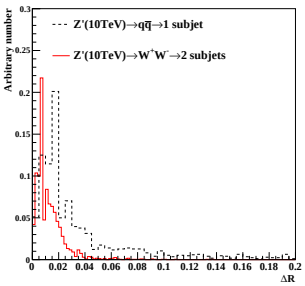


(i) The fourth trailing-T

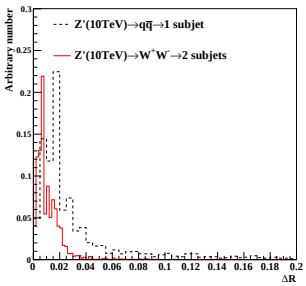


(j) The fifth trailing-T

Figure 27: Distributions of $\Delta R$ for $M(Z') = 10$ TeV for five kinds of trailing particles with the reco-level information of ECAL are shown here.

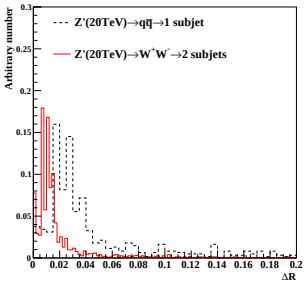


(a) The first trailing-PT

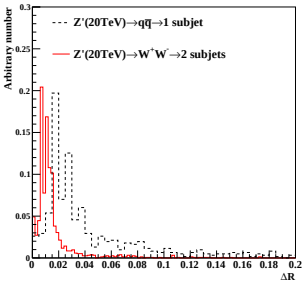


(b) The second trailing-PT

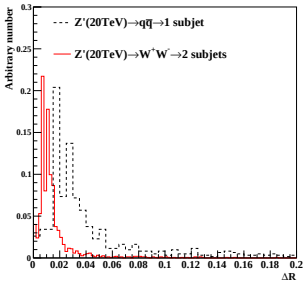


(c) The third trailing-PT

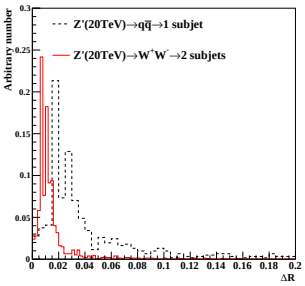


(d) The fourth trailing-PT

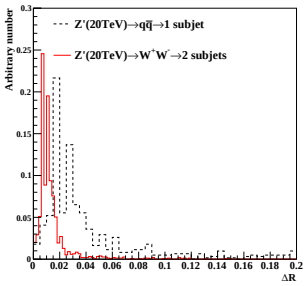


(e) The fifth trailing-PT

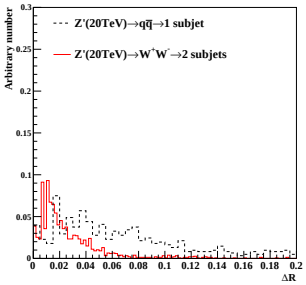


(f) The first trailing-T

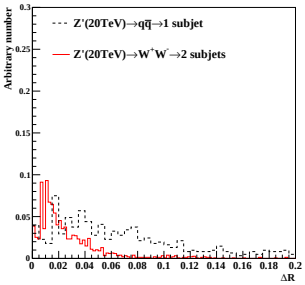


(g) The second trailing-T

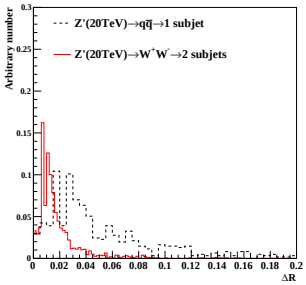


(h) The third trailing-T

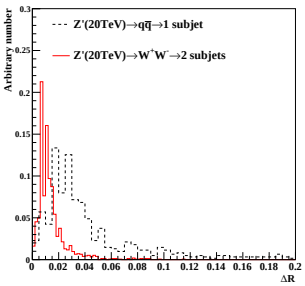


(i) The fourth trailing-T

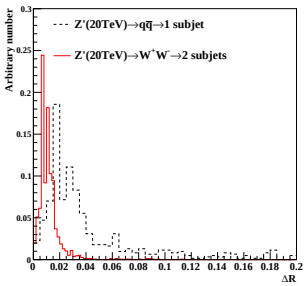


(j) The fifth trailing-T

Figure 28: Distributions of $\Delta R$ for $M(Z') = 20$ TeV for five kinds of trailing particles with the reco-level information of ECAL are shown here.

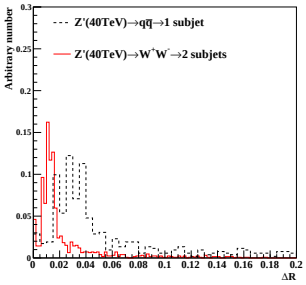


(a) The first trailing-PT

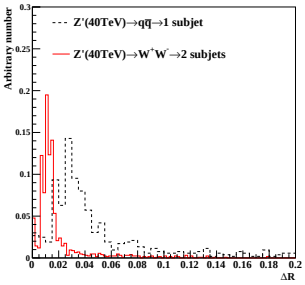


(b) The second trailing-PT

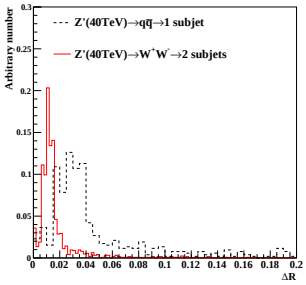


(c) The third trailing-PT

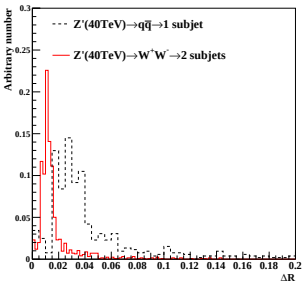


(d) The fourth trailing-PT

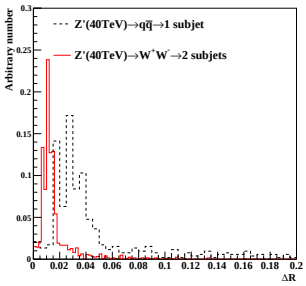


(e) The fifth trailing-PT

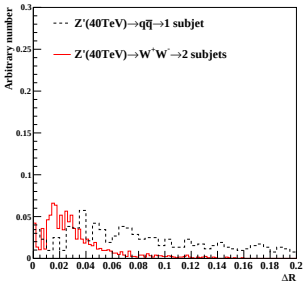


(f) The first trailing-T

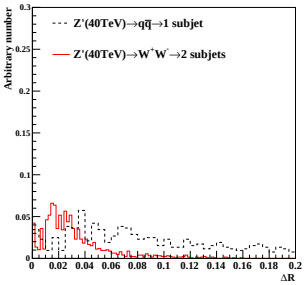


(g) The second trailing-T

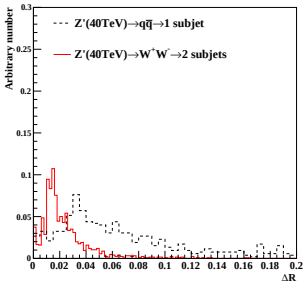


(h) The third trailing-T

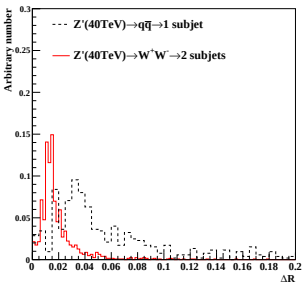


(i) The fourth trailing-T

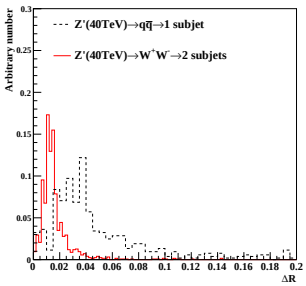


(j) The fifth trailing-T

Figure 29: Distributions of $\Delta R$ for $M(Z') = 40$ TeV for five kinds of trailing particles with the reco-level information of ECAL are shown here.